Journal of Power Sources 235 (2013) 111–116

Contents lists available at SciVerse ScienceDirect

Journal of Power Sources

journal homepage: www.elsevier.com/locate/jpowsour

A study towards superior carbon nanotubes-supported Pd-based catalysts for formic acid electro-oxidation: Preparation, properties and characterisation

Marjan Marinšek [a,*], Martin Šala [b], Boštjan Jančar [c]

[a] University of Ljubljana, Faculty of Chemistry and Chemical Technology, Aškerčeva 5, 1000 Ljubljana, Slovenia
[b] National Institute of Chemistry, Hajdrihova 19, SI-1001 Ljubljana, Slovenia
[c] Jožef Stefan Institute, Jamova 39, 1000 Ljubljana, Slovenia

HIGHLIGHTS

- The influence of experimental parameters on morphology of catalyst was investigated.
- Homogeneous and heterogeneous precipitation of Pd was achieved.
- Smaller particle size of catalyst show higher specific current densities.

ARTICLE INFO

Article history:
Received 25 October 2012
Received in revised form
4 January 2013
Accepted 4 February 2013
Available online 16 February 2013

Keywords:
Pd/C catalysts
Preparation
Morphology
Formic acid electro-oxidation

ABSTRACT

This study investigates several CNT-supported Pd-based catalysts and compares their morphological as well as electrochemical characteristics for formic acid electro-oxidation. Pd/C catalysts are prepared via various impregnation methods, using different reaction media or reducing agents. The average mean particle sizes of the precipitated Pd vary from 2.6 nm to 18.0 nm. It is further shown that the particle size of Pd/C dispersions can be easily controlled by changing the solvent and experimental conditions during the preparation procedure. Measurements of catalytic activity by using cyclic voltammetry reveal strong particle size dependence of the anodic peak current density. The electro-oxidation of formic acid may be kinetically-controlled or diffusion-controlled regarding the Pd morphological characteristics.

1. Introduction

Recently, direct formic acid fuel cells (DFAFC) have been studied and considered as promising power sources for portable electronic devices and electric vehicles. When compared to H_2-PEMFCs (H_2-fed polymer electrolyte membrane fuel cells) or DMFCs (direct methanol fuel cells), DFAFCs have many advantages. They are characterised by high electromotive force, limited fuel crossover rate through the Nafion membrane due to the electrostatic repulsion between $HCOO^-$ in SO_3^- ions in the Nafion membrane, and have high practical power densities at low temperatures since the optimal operating concentration of formic acid (FA) can be as high as 20 mol L^{-1}, while the optimal concentration of methanol in DMFC is only 2 mol L^{-1} [1–5].

FA is electrochemically oxidised in DFAFC on the anode side on the catalyst surface. For the electro-oxidation of formic acid at relatively low temperatures, Pd- or Pd/Me-nano-particles have been examined due to Pd superb FA electro-oxidation promotion when compared to Pt-based catalysts. In order to reduce the Pd loading, the only practical means of doing so in DFAFC systems are carbon-supported catalysts. In addition to the active catalyst component, the choice of suitable carbon support, particularly for electro-catalysts, is also an important factor for the catalytic activity performance, as the interaction between Pd-catalysts and carbon support could affect the catalytic activities. Recently, carbon nanotubes (CNTs) have been considered as a promising catalyst support material. The tubular structure of CNTs makes them unique among different forms of carbon. CNTs exhibit relatively high surface areas, excellent electronic conductivity, and high chemical stability [6].

It was reported that the catalytic activity of Pd-based catalysts depends strongly on the size, shape and size distribution of the metal particles, in addition to their dispersion on the support [7–

* Corresponding author. Tel.: +386 1 2419 204.
E-mail addresses: marjan.marinsek@fkkt.uni-lj.si (M. Marinšek), martin.sala@ki.si (M. Šala), bostjan.jancar@ijs.si (B. Jančar).

0378-7753/$ – see front matter © 2013 Elsevier B.V. All rights reserved.
http://dx.doi.org/10.1016/j.jpowsour.2013.02.020

12]. Generally, the smaller the Pd-particles, the more enhanced the electro-catalytic activity for formic acid oxidation. Though many facts regarding the beneficial geometric and electronic effects of the Pd-based catalysts are already known, a more detailed mechanistic understanding of formic acid electro-oxidation is still needed for the rational design of the catalysts. In this respect, the Pd-particle size effect of formic acid electro-oxidation has to some extent already been discussed. The change in specific catalysts' activity with Pd-particle size was rationalised by binding energy shifts and D-band vacancy changes [28]. Generally, in terms of beneficial particle size effects, 5–7 nm Pd-nanoparticles were reported to be the most favourable for formic acid electro-oxidation [11].

There are several methods of synthesising supported Pd-catalysts for DFAFCs, including the impregnation method by chemical or electrochemical reduction [7,13–18], the micro-emulsion method [19,20], the colloidal method [21,22], ion-exchange [23] and thermal decomposition [24]. An impregnation method is particularly interesting for the synthesis of carbon-supported Pd-catalysts due to its simplicity and the possibility of preparing nano-sized precipitates of controlled size distribution. Many experimental factors affect the morphology and distribution of the metal particles on the catalyst support in the impregnation process, such as the nature of the carbon support and the metal precursor used, the chemical reduction method, the reaction time, the reaction media and the use of surfactant agent or stabilising polymer molecules [13,25].

This study investigates the characteristics of CNT-supported Pd-catalysts for FA electro-oxidation. The catalysts have been prepared by various impregnation routes and subsequently compared in terms of their morphological characteristics and the ability for FA oxidation.

2. Experimental procedure

2.1. Catalyst preparation

Pd/CNTs dispersions were prepared by various impregnation methods using different reaction media or/and reducing agents as summarised in Table 1.

Catalysts S1–S5: In a typical preparation procedure, 20.0 mg of CNTs (MWCNTs Baytubes, Bayer, >95% C-purity) were suspended under sonication in 5.0 mL of various reaction media (ethanol, >99.5%, Merck; methanol, >99.5%, Merck; THF, >99%, Merck). Separately, 15.0 mg of palladium (II) acetate (>99%, Acros) was dissolved in 5.0 mL of the previously chosen solvent and then added into the CNT suspension. Thus prepared mixture was further sonicated for 30 min. After sonication, a freshly prepared hydroquinone solution in the previously chosen solvent (5.0 mL, 0.5 M) was admixed to trigger the reduction of Pd^{2+} ions. The reduction reaction was instantaneous; however, the reaction mixture was further kept in the mother solution and mixed for prolonged time (t_r). Afterwards, the reaction mixture was filtered through a 0.2 μm PTFE membrane filter, washed with the originally chosen solvent, and dried under vacuum at room temperature.

Table 1
Preparation data for various Pd–C catalysts.

Sample	Reaction media	Reducing agent	t_r/h
S1	Ethanol	Hydroquinone	2
S2	Ethanol	Hydroquinone	48
S3	Methanol	Hydroquinone	2
S4	THF	Hydroquinone	2
S5	THF	Hydroquinone	48
S6	H_2O	SDS	6

Catalyst S6: This material was prepared using a slight modification of an experimental procedure published by Karousis et al. [26] 20.0 mg of CNTs (MWCNTs Baytubes, Bayer, >95% C-purity) were suspended in 40.0 mL of 0.05 M aqueous SDS (Dodecyl sulphate, sodium salt, Aldrich, >98%) solution and sonicated for 60 min. After sonification, 40.0 mg of palladium (II) acetate (Acros, >99%) was added into the reaction mixture and dissolved during vigorous mixing. SDS played double role in this experiment. As a surfactant, it covers the CNT surface, and after conversion to 1-dodecanol it acts as a reduction agent. The reaction mixture was then heated and kept boiling under reflux for 8 h to reduce Pd^{2+} ions and decorate CNTs with Pd-nanoparticles. After cooling, the reaction mixture was filtered through a 0.2 μm PTFE membrane filter, washed extensively with water to remove residual surfactant SDS and dried under vacuum at room temperature. MiliQ water was used throughout the work.

2.2. Catalysts characterisation

The electrochemical oxidation of formic acid on the prepared catalysts was studied via a cyclic voltammetry (CV) method at room temperature (23 ± 1 °C). A Princeton Applied Research potentiostat/galvanostat (EG&G model 273) was used for the electrochemistry measurements in a conventional three-electrode electrochemical cell. The working electrode was a thin layer of Nafion-impregnated catalyst cast on a glassy carbon (GC) disc with diameter of 5 mm (electrode area 0.196 cm^2) held in a Teflon cylinder. A Pt-wire and an Ag/AgCl electrode (in saturated KCl) were used as the counter and reference electrodes, respectively (all potentials in this paper are quoted versus the Ag/AgCl reference). To keep the metal loading for all investigated Pd/C dispersions constant the catalyst layer on the glassy carbon working electrode was obtained in the following way: ca. 5–10 mg of the Pd/C catalyst was dispersed ultrasonically in 3 mL of isopropanol with 12 μL of 5 wt% Nafion solution (Aldrich) to obtain a homogeneous ink. 10–15 μL of the ink was then dropped by a micropipette and spread onto the top surface of the mirror-polished GC disc. Finally, the electrode was dried at room temperature overnight. Based on the geometric area of the GC disc the catalyst loading was ca. ~25–39 μg_{Pd} cm^{-2}. The base CV experiments were carried out in 0.5 M H_2SO_4 solution, which was de-aerated with ultra-high-purity nitrogen before each experiment. Prior to measuring the CVs, the working electrode was electrochemically cleaned in base electrolyte via 150 CV cycles. For the examination of the activity of the formic acid oxidation on the catalysts, the measurement was carried out in the de-aerated electrolyte of 0.5 M H_2SO_4 containing also 0.5 M HCOOH. The electrolyte solutions were prepared from high purity sulphuric acid, high purity formic acid and MQ water. CV curves were collected at a scan rate 50 mV s^{-1}. The reported CV curves of FA electro-oxidation were taken after ~20 min of catalysts cycling in H_2SO_4 + HCOOH electrolyte.

Particle size and morphology observations of the prepared Pd/C dispersions were performed on a JEOL JEM-2100 transmission electron microscope (TEM) operated at 200 kV, which was equipped with EDX. TEM samples were prepared by dispersing the powders in ethanol using ultra-sonification followed by the deposition of the obtained suspension on holey carbon-coated copper grids. Quantitative image analyses were performed on the obtained digital images (images were digitised into pixels with 255 different grey values using Zeiss KS300 3.0 image-analysis software). For statistically reliable data in each case, 5–10 different regions were analysed.

To determine the practical amount of Pd in the prepared Pd/C dispersions, samples were submitted to thermo-gravimetric (TG) investigation using the Mettler TA4000 instrument. In a typical TG test, the Pd/C catalyst was treated in the temperature range of 30–

900 °C at a constant flow of Ar–O_2 (18 L h^{-1}) to burn out the C-support. The residue corresponds to pure Pd.

Specific surface area by nitrogen adsorption (BET) of the prepared Pd/C catalysts were determined using Micromeritics ASAP 2020 system.

3. Results and discussion

The TEM images together with the corresponding particle size distribution histograms of the prepared catalysts are represented in Fig. 1. It is evident that the experimental parameters during the catalyst preparation influence the morphology of Pd/C dispersions significantly. Relatively small Pd-nanoparticles (dark grey dots in TEM images) with homogeneous Pd distribution over C-support (light grey base in TEM images) are prepared in ethanol (Fig. 1a). Two hours (t_r) of system mixing after the addition of hydroquinone results in Pd-nanoparticles with an average particle size 4.8 nm. Several small Pd-nanoparticles further merge into agglomerates, typically 10–20 nm in size. However, these agglomerates are rather 2-D structures on the C-substrate (as shown in small STEM image in Fig. 1a), meaning that the Pd-surface remains mostly opened. The prolonged time t_r of system mixing clearly increases the average agglomerate size (6.5 nm) without increasing the decoration of C-support with Pd-precipitates (Fig. 1b). Moreover, the Pd-agglomerates grow into 3-D structures reducing the available Pd-surface. When compared to ethanol, methanol as the reaction media under identical reaction conditions provides fairly larger Pd-precipitates with less uniform size distribution (Fig. 1c). Larger Pd-precipitates at similar Pd-loading also result in lower coverage of the C-support. Since Pd-precipitates in methanol grow up to several tens of nanometres in diameter (the average particle size 18.0 nm) already at $t_r = 2$ h longer mixing times t_r are omitted. When the solvent is changed to THF, the Pd particle size is decreased distinctly, exhibiting an average value 4.1 nm (Fig. 1d). The Pd-loading on C-support is relatively uniform without any larger agglomerates. Increasing t_r in the case of THF reaction media rises the Pd-loading, though some Pd agglomeration is also noticed (Fig. 1e). In all three cases, when organic solvents are used as the reaction

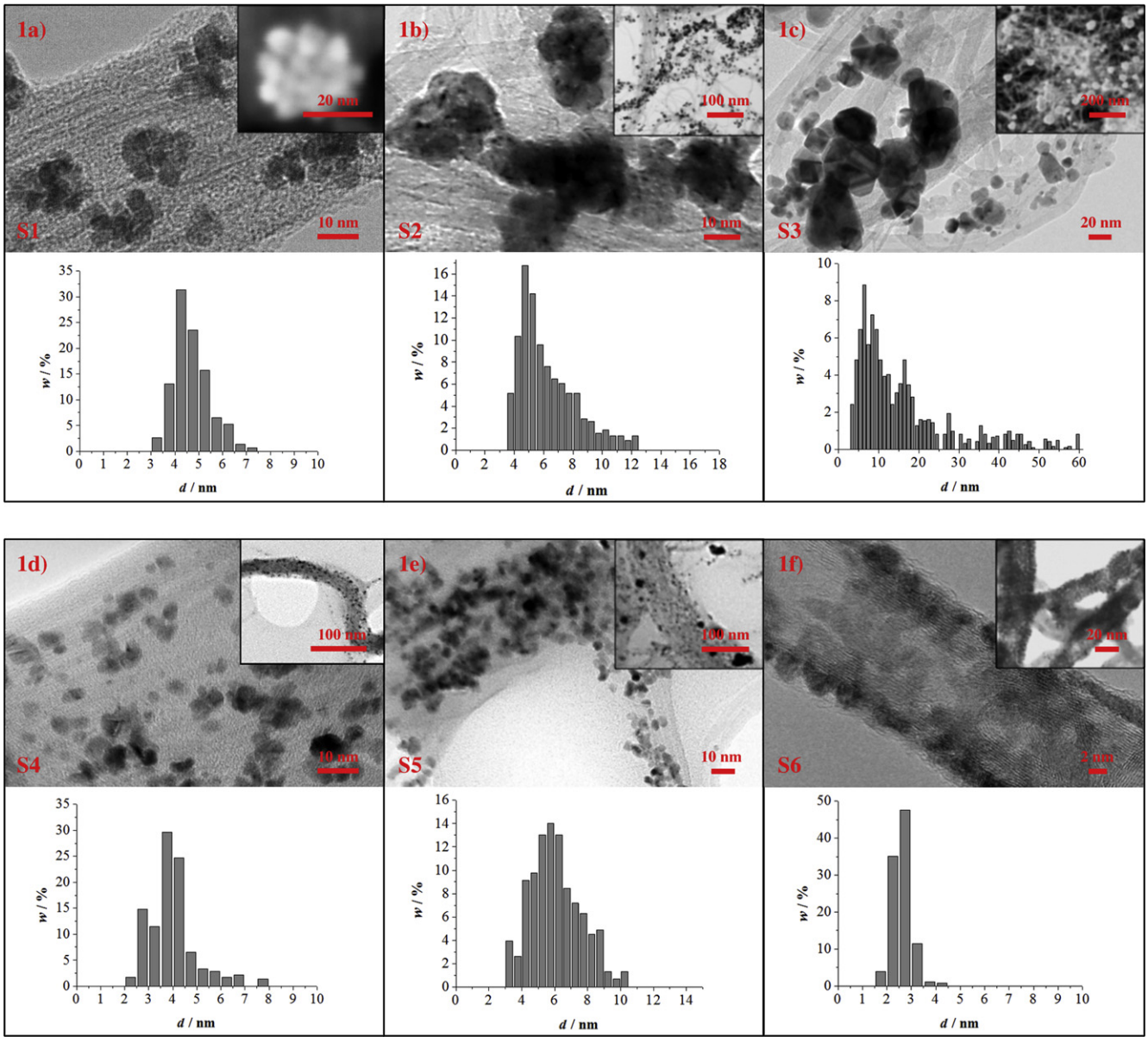

Fig. 1. TEM micrographs and the corresponding size distribution histograms of various Pd/C catalysts.

media, the mixing of Pd-source and reducing agent in solution causes homogeneous precipitation of Pd in the whole reaction volume. Since hydroquinone triggers rapid nucleation, the newly formed solid Pd-phase remains as nano-precipitates. The precipitated Pd-nanoparticles, which in time slowly agglomerated, are then adsorbed on the C-surface. Such a mechanism results in increased Pd-loading on the C-surface over time and is clearly demonstrated in the case of S1–S2 and S4–S5 samples (Table 2).

In contrast, significant improvement regarding the decoration of C-support with Pd-nanoparticles is achieved by replacing the organic solvent with aqueous reaction media and introducing the SDS surfactant (Fig. 1f). In this case, the distribution of Pd-nanoparticles is remarkably uniform, with practically full coverage of MWCNTs. The precipitated Pd-nanoparticles are of very narrow size distribution with an average particle size of 2.6 nm. Keeping the prepared Pd/C dispersion in the mother suspension for a prolonged time does not change its morphological characteristics. Such superb Pd decoration of MWCNTs in the latter case may be ascribed to the fact that the reaction parameters favour heterogeneous precipitation of Pd. According to the literature [26], SDS is first adsorbed on the MWCNTs surface, then over time thermally converted into 1-dodecanol, which triggers the reduction of Pd^{2+} ions in many active sites directly on the MWCNTs' surface.

Table 2 summarises the total surface area A_{total}, the Pd-loading w_{Pd} and reaction yield ζ (calculated as Pd content in the final product vs. theoretical Pd content), as well as the electrochemically active surface area (ECSA) of the six prepared Pd/C catalysts. The highest Pd-loading on C-support and reaction yield are achieved in the case of Sample 6 (40.6% and 83.42%, respectively). Prolonged reaction time t_r increases the reaction yield (S1–S2 and S4–S5 samples); however, due to Pd-agglomeration, it also decreases the surface area of the catalysts. Pd-particle size and the degree of their agglomeration are furthermore reflected through the active surface area measurements. In general, it is fundamentally important to grow the metal seeds uniformly into small particles for the purpose of obtaining a large active surface area.

Fig. 2 shows a comparison of CV data for the various Pd/C catalysts immersed in 0.5 M H_2SO_4 with a sweep rate of 50 mV s^{-1}. According to Fig. 2, all electro-catalysts show the expected behaviour in H_2SO_4 solution with characteristic and well-defined hydrogen adsorption/desorption peaks around 0 V, the formation of PdO_x at higher potentials in the forward scan, and a PdO_x reduction peak in the reverse scan at ca. 0.4–0.5 V. The described features of measured CV curves agree well with the reported data in the literature [27–32]. The main differences between the CVs are in the double layer capacitance, which is for some Pd/C catalysts substantially higher, and in the position of the PdO_x reduction peak. PdO_x reduction is in the case of sample S6 shifted positively (0.43 V), relative to the peak reduction potential of the S1 and S4 samples (0.382 V and 0.380 V, respectively). The positive shift of the reduction potential indicates the reduced oxophilicity and weakened chemisorption with oxygen-containing species (i.e. OH_{ad}) on Pd-surface. Since the hydrogen adsorption/desorption on Pd may be overlapped by hydrogen adsorption/dissolution [34] in Pd, we

Table 2
Physical properties of various Pd–C catalysts.

Sample	w_{Pd} in the Pd/C/%	ζ/%	A_{total}/m^2 g^{-1}	ECSA/m^2 $g^{-1}{}_{Pd}$
S1	14.8	56.45	129.4	62
S2	17.9	68.63	119.1	13
S3	15.5	59.12	110.5	10
S4	14.8	56.45	123.3	59
S5	16.4	62.55	116.1	28
S6	40.6	83.42	144.3	86

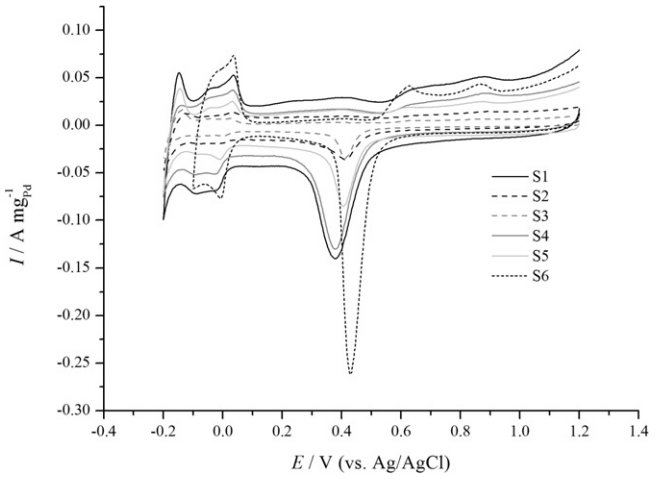

Fig. 2. CVs of various Pd/C catalysts in 0.5 M H_2SO_4 with a scan rate 50 mV s^{-1}.

calculated the ECSA of the prepared catalysts, taking into account the charge consumed during the PdO_x reduction in the course of the cathodic scan and using the value of 0.424 mC cm^{-2} as charge consumed for monolayer oxide reduction (Table 2). Such procedures are well established in the literature [33–35]. The calculated ECSA values can provide important information on the available active sites on catalysts. The relatively higher ECSA values of samples S1, S4 and S6 in comparison with S2, S3 and S5 samples confirm the better dispersion and smaller particle size of Pd decoration over C-support in former case.

The obtained Pd/C catalysts were employed to catalyse FA oxidation reaction in sulphuric acid solution; the results are shown in Fig. 3. During the forward scan, all the catalysts show the main peak for formic acid oxidation in the potential range between 0.25 V and 0.4 V. This peak corresponds to the oxidation of formic acid through the direct mechanism (deprotonation pathway) [36]. In contrast, a second broad peak at higher potentials (0.5–0.6 V) adjacent to the first peak is also visible. Due to the position of the later peak, it could be attributed to the oxidation of adsorbed CO requiring an additional over-potential for CO_2 formation [37,38]. Such a pattern of CV curves suggests that the mechanism tentatively proposed for the electro-oxidation of formic acid on Pd-

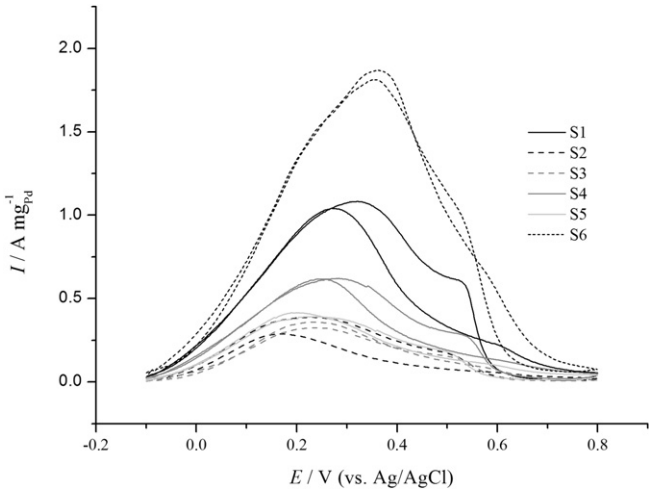

Fig. 3. Cyclic voltammetry data for various Pd/C catalysts immersed in 0.5 M H_2SO_4 + 0.5 M HCOOH at a scan rate 50 mV s^{-1}.

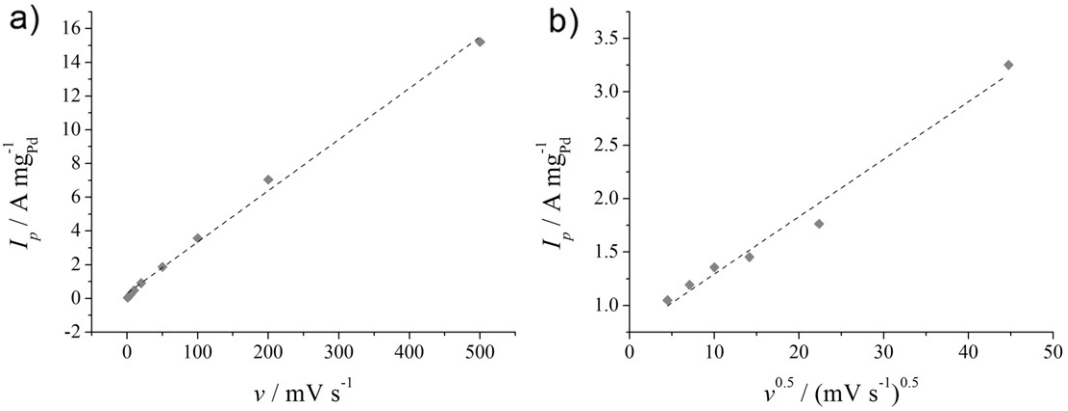

Fig. 4. Dependence of peak current density I_p on scan rates v for samples S6 (a) and S1 (b).

catalyst is based on two parallel pathway processes [39]: i) a "direct pathway" involving a formate anion possibly bound to Pd via CH-activation, and ii) an "indirect pathway" based on dehydrogenation of HCOOH and absorption of CO on Pd-surface. Based on a relatively large current hysteresis loop in the positive-direction vs. negative-going potential scans, where with negative-going potential scan the peak current density is higher and located at higher potentials, we further corroborate that FA is partially oxidised by the indirect pathway mechanism. The absorbed CO can be oxidised to CO_2 on the Pd-surface at relatively higher potentials during negative-going potential scan. Since the CV patterns in H_2SO_4 + HCOOH electrolyte does not change with consecutive cycles, we may conclude that the prepared Pd/C catalysts exhibit a very good tolerance towards CO poisoning. The current densities in the positive-direction scan for S1–S6 catalysts are measured as 1.083 A mg$^{-1}_{Pd}$, 0.287 A mg$^{-1}_{Pd}$, 0.359 A mg$^{-1}_{Pd}$, 0.621 A mg$^{-1}_{Pd}$, 0.390 A mg$^{-1}_{Pd}$ 1.867 A mg$^{-1}_{Pd}$, respectively, and may be correlated to the calculated ECSA or mean particle size values. Smaller particles with lower mean particle size and higher ECSA values exhibit fairly higher specific current densities. In this respect, the outstanding catalytic activity of the catalyst S6 is mainly due its higher specific area of Pd/C catalyst, which originates from the smaller Pd-nanoparticles size and superb dispersion on the C-support. However, the rather high performance of the S6 catalyst can be achieved only by carefully washing it after the synthesis and in particular electrochemical cleaning by potential cycling, both to remove the adsorbed surfactant SDS from the Pd-surface. Any residuals on the Pd-surface may substantially limit the catalytic activity because of blocking the surface active sites. We found that at least 150 potential cycles in the range from 1.2 to −0.1 V are necessary to clean the catalyst surface and to achieve stable and repeatable CV responses. The above results of FA electro-oxidation clearly demonstrate a significant influence of Pd particle size on measured catalyst activity.

In order to investigate a partial kinetic characterisation of FA electro oxidation on S1 and S6 catalysts, the effects of scan rate v and FA concentration C_{HCOOH} on the anodic peak current density I_p during the forward scans were measured (Figs. 4 and 5). According to the results in Fig. 4, the anodic peak current density is linearly proportional to the scan rates in the case of sample S6. In contrast, the I_p vs. v relationship for the S1 sample exhibit square root dependence. Both relationships imply that FA electro oxidation may be kinetically-controlled or diffusion-controlled for samples S6 and S1, respectively. Regarding the chosen electrolyte concentration such dependences may be explained through different morphological characteristic of both samples. In the case of the S6 sample, C-support is decorated with non-agglomerated Pd-nanoparticles, making all Pd-surfaces available for the surrounding FA. The formation of 2-D agglomerated Pd-clusters in the S1 sample, on the other hand, still ensures a fairly open Pd-surface; however, the access of the reagent FA to the active catalyst sites is to some extent hindered.

The effect of C_{HCOOH} on the I_p for sample S6 is shown in Fig. 5. It is clear that the anodic peak current density increases with the increasing FA concentration approaching some limiting value.

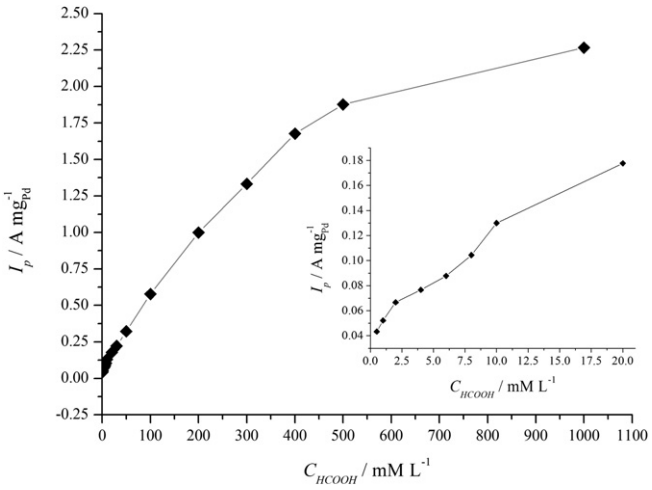

Fig. 5. Peak current density I_p as a function of FA concentration C_{HCOOH} at a scan rate v 50 mV s^{-1} for samples S6 (small inset enlarges I_p vs. C_{HCOOH} dependence at relatively low FA concentrations).

4. Conclusions

Several Pd/C dispersions were prepared with various impregnation routes and subsequently compared in terms of their morphological characteristics and the ability for FA oxidation. It was demonstrated that the experimental parameters during the catalyst preparation very much influence the morphology of Pd/C dispersions. An organic solvent as a reaction media with dissolved reducing agent triggered homogeneous precipitation of Pd in the whole reaction volume, lowering the Pd content in the final product. In contrast, by replacing the organic solvent with aqueous reaction media and introducing the SDS surfactant, uniform decoration of C-support with Pd-nanoparticles as well as higher Pd content in the final product were achieved. In this case, the distribution of Pd-nanoparticles was remarkably uniform, with practically full coverage of MWCNTs.

The calculated ECSA values of the Pd/C dispersions during the electrochemical tests were in accordance with the results of the morphological characteristics as observed with TEM. Lower mean particle sizes of the deposited Pd ensured higher ECSA values. The Pd particle size influence was also observed for FA electro-oxidation where smaller particles with lower mean particle size and higher ECSA values exhibited fairly higher specific current densities. It was also observed that the I_p vs. v relationship may follow linear (kinetically-controlled) or square root (diffusion-controlled) dependence. Such a diverse relationship was ascribed to various Pd-agglomeration degrees. The non-agglomerated Pd-nanoparticles made all Pd-surfaces available for the surrounding FA, making its electro-oxidation kinetically-controlled. With the formation of 2-D agglomerated Pd-clusters, the access of the surrounding FA to the active catalyst sites was to some extent hindered resulting in diffusion-controlled FA electro-oxidation.

Acknowledgements

We are thankful for the financial contribution of the Ministry of Higher Education, Science and Technology of the Republic of Slovenia through grant P1-0175-103 and Center of Excellence Low-Carbon Technologies (CO NOT).

References

[1] X. Wu, P.G. Pickup, J. Power Sources 182 (2008) 124–132.
[2] Y. Zhu, S. Ha, R.I. Masel, J. Power Sources 130 (2004) 8–14.
[3] F. Garin, Catal. Today 89 (2004) 255–268.
[4] R. Larsen, S. Ha, J. Zakzeski, R.I. Masel, J. Power Sources 157 (2006) 78–84.
[5] Y.W. Rhee, S. Ha, R.I. Masel, J. Power Sources 117 (2003) 35–38.
[6] M. Carmo, V.A. Paganin, J.M. Rosolen, E.R. Gonzales, J. Power Sources 142 (2005) 169–176.
[7] M.S. Nashner, A.I. Frenkel, D.L. Adler, J.R. Shapley, R.G. Nuzzo, J. Am. Chem. Soc. 119 (1997) 7760–7771.
[8] I.S. Armadi, Z.L. Wang, T.C. Green, A. Henglein, M.A. El-Sayed, Science 272 (1996) 1924–1925.
[9] W.P. Zhou, A. Lewera, R. Larsen, R.I. Masel, P.S. Bagus, A. Wieckowski, J. Phys. Chem. B 110 (2006) 13393–13398.
[10] H. Li, G. Sun, Q. Jiang, M. Zhu, S. Sun, Q. Xin, Electrochem. Commun. 9 (2007) 1410–1415.
[11] W. Zhou, J.Y. Lee, J. Phys. Chem. 112 (2008) 3789–3793.
[12] R.K. Pandey, V. Lakshminarayanan, J. Phys. Chem. C 113 (2009) 21596–21603.
[13] Y. Huang, J. Liao, C. Liu, T. Lu, W. Xing, Nanotechnology 20 (2009) 105604.
[14] C.W. Hills, N.H. Mack, R.G. Nuzzo, J. Phys. Chem. B 107 (2003) 2626–2636.
[15] M. Tristany, J. Courmarcel, P. Dieudonne, M. Moreno-Manas, R. Pleixats, A. Rimola, M. Sodupe, S. Villarroya, Chem. Mater. 18 (2006) 716–722.
[16] S. Rather, R. Zacharia, S.W. Hwang, M. Naik, K.S. Nahm, Chem. Phys. Lett. 441 (2007) 261–267.
[17] T.M. Day, P.R. Unwin, J.V. Macpherson, Nano Lett. 7 (2007) 51–57.
[18] T.T. Cheng, E.L. Gyenge, J. Appl. Electrochem. 39 (2009) 1925–1938.
[19] Y. Liu, X. Qiu, Z. Chen, W. Zhu, Electrochem. Commun. 4 (2002) 550–553.
[20] W. Xu, T. Lu, C. Liu, W. Xing, J. Phys. Chem. B 109 (2005) 14325–14330.
[21] Y. Huang, X. Zhou, J. Liao, C. Liu, T. Lu, W. Xing, Electrochem. Commun. 10 (2008) 621–624.
[22] C. Bock, C. Paquet, M. Couillard, G.A. Botton, B.R. MacDougall, J. Am. Chem. Soc. 126 (2004) 8028–8037.
[23] A. Sartre, M. Phaner, L. Porte, G.N. Sauvion, Appl. Surf. Sci. 70–71 (1993) 402–406.
[24] B. Xue, P. Chen, Q. Hong, J. Lin, K. Lee, K. Tan, J. Mater. Chem. 11 (2001) 2378–2381.
[25] A.J. Dickinson, L.P.L. Carrette, J.A. Collins, K.A. Friedrich, U. Stimming, Electrochim. Acta 47 (2002) 3733–3739.
[26] N. Karousis, G.E. Tsotsou, F. Evangelista, P. Rudolf, N. Ragoussis, N. Tagmatarchis, J. Phys. Chem. C 112 (2008) 13463–13469.
[27] M. Chen, Z.B. Wang, K. Zhou, Y.Y. Chu, Fuel Cells 10 (2010) 1171–1175.
[28] H. Duncan, A. Lasia, Electrochim. Acta 52 (2007) 6195–6205.
[29] Y.W. Lee, J.K. Oh, H.S. Kim, J.K. Lee, S.B. Han, W. Choi, K.W. Park, J. Power Sources 195 (2010) 5896–5901.
[30] B.Y. Zhu, Y. Kang, Z. Zhu, Q. Zhu, J. Zheng, B. Xia, H. Yang, Fuel Cells Bull. 2008 (2008) 12–15.
[31] Y.N. Wu, S.J. Liao, Y.L. Su, J.H. Zeng, D. Dang, J. Power Sources 195 (2010) 6459–6462.
[32] S. Yang, X. Zhang, H. Mi, X. Ye, J. Power Sources 175 (2008) 26–32.
[33] T.R. Soreta, J. Strutwolf, O. Henry, C.K. OSullivan, Langmuir 26 (2010) 12293–12299.
[34] I. Park, K. Lea, S. Yoo, Y. Cho, Y. Sung, Electrochim. Acta 55 (2010) 4339–4345.
[35] T. Cochell, A. Manthiram, Langmuir 28 (2012) 1579–1587.
[36] Z. Liu, L. Hong, M.P. Tham, T.H. Lima, H. Jiang, J. Power Sources 161 (2006) 831–835.
[37] T. Maiyalagan, Abu Bakr A. Nassr, T.O. Alaje, M. Bron, K. Scott, J. Power Sources 211 (2012) 147–153.
[38] W. Lu, W. Chen, J. Phys. Chem. C 114 (2010) 21190–21200.
[39] N. Chen, H. Lv, W. Wang, S. Mu, M. Pan, F. Marken, J. Power Sources 195 (2010) 7246–7249.